Scalable Biosynthetic Production of Knotted Peptides Enables ADME and Thermodynamic Folding Studies

Christopher J. Schwalen, Charles Babu, Swastik Phulera, Qin Hao, Daniel Wall, David O. Nettleton, Tejas P. Pathak,* and Piro Siuti*

Read Online

ACCESS | Metrics & More | Article Recommendations | Supporting Information

ABSTRACT: Knotted peptides present a wealth of structurally diverse, biologically active molecules, with the inhibitor cystine knot/knottin class among the most ecologically common ones. Many of these natural products interact with extracellular targets such as voltage-gated ion channels with exquisite selectivity and potency, making them intriguing therapeutic modalities. Such compounds are often produced in low concentrations by intractable organisms, making structural and biological character-ization challenging, which is frequently overcome by various expression strategies. Here, we sought to test a biosynthetic route for the expression and study of knotted peptides. We screened expression constructs for a biosynthesized knotted peptide to determine the most influential parameters for successful disulfide folding and used NMR spectroscopic fingerprinting to validate topological structures. We performed pharmacokinetic characterization, which indicated that the interlocking disulfide structure minimizes liabilities of linear peptide sequences, and propose a mechanism by which knotted peptides are cleared. We then developed an assay to monitor solution folding in real time, providing a strategy for studying the folding process during maturation, which provided direct evidence for the importance of backbone organization as the driving force for topology formation.
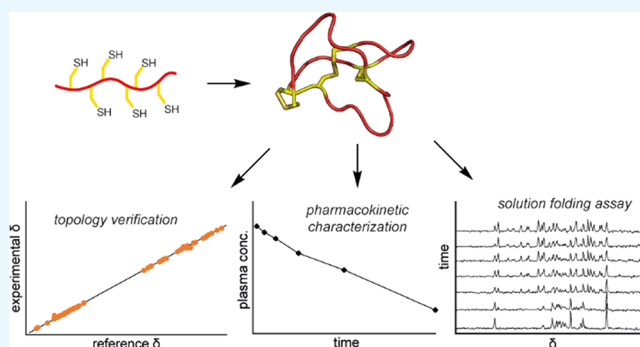
INTRODUCTION

Ribosomal peptides are highly modular natural products, and post-translational modifications can introduce additional structural modifications, altering function and further elabo-rating on the canonical amino acid diversity.[1] One prolific role of peptides in the natural world is as components of venom cocktails—mixtures of peptides that evolved to interrogate cell surface receptors in a specific, potent, and rapid manner for animal defense or predation.[2] While these mixtures contain a staggering sequence diversity of toxins, they consistently make use of interlocking disulfide bonds to create a rigid topology.[3] Due to their ability to selectively modulate pharmacologically relevant targets and remain stable with a high apparent level of sequence tolerance, knotted peptides have attracted interest as both therapeutic compounds and as scaffolds for epitope grafting or as molecular targeting motifs (Figure 1).[4−8] Despite promise, many characteristics of disulfide-rich venom (DRV) scaffolds remain unclear, including pharmacokinetic (PK) properties and how the knotted disulfide bonds form. Moreover, strategies for chemical and biosynthesis vary widely,[9−13] often lacking consensus methodology, structural characterization, and justification for chosen parameters.

Here, we tested parameters that influence correct topology expression and validate production of different sequences by nuclear magnetic resonance (NMR) spectroscopy finger-printing to confirm that the biosynthesized compounds replicate the folding present in natively produced sequences and utilize chemical refolding to minimize isomer formation. PK analysis was performed for a validated DRV sequence to determine the role of the knotted structure in in vivo properties. Lastly, a real-time folding assay was developed, which was used to determine the mechanism by which this conformation forms in solution, providing a method for study for this diverse family of compounds.
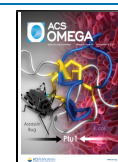
RESULTS AND DISCUSSION

Thioredoxin Tag Optimally Balances Yield and Disulfide Oxidation. While there are multiple examples of prokaryotic DRV expression, there is little consensus on methodology and characterization efforts.[11,12,14,15] We sought to understand how select expression parameters influence
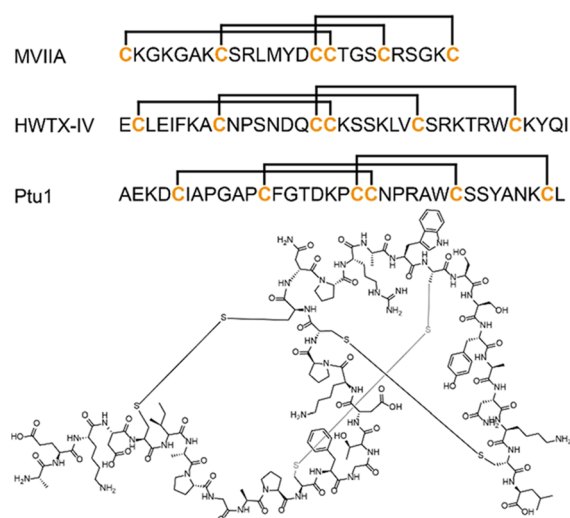
Figure 1. Examples of compounds with knotted disulfide structures. Structure of Ptu1 highlights the topology endowed by interlocking disulfide bonds.

peptide maturation outcomes. We began by assembling constructs of fusion tags and *Escherichia coli* expression strains to evaluate combinations on yield, purity, and peptide oxidation, assessed by gel electrophoresis, absorbance spectroscopy, and liquid chromatography−mass spectrometry (LC−MS, Figure S1, Figure 2). Tobacco etch virus (TEV) protease was chosen to remove the N-terminal fusion tag because of its specificity toward its recognition motif, allowing its use irrespective of the DRV sequence; its cleavage retains an additional N-terminal Gly residue, present in all of the compounds produced here. Constructs for expression of the DRV Ptu1, which was originally isolated from the assassin bug *Peirates turpis* and to our knowledge has not been recombinantly biosynthesized, were constructed (Tables S2−S4).[16] In contrast with studies producing related cyclotides and cyclic DRVs, which are cyclized N- to C-terminus via split-inteins,[17−19] tags selected here could also play a nonstructural role, for example, shuttling DRV to periplasm for oxidation (Table S3). Hence, fusion partner tags to the peptide included solubilizing partners [cytoplasmic maltose binding protein (cMBP), thioredoxin (Trx), glutathione S-transferase (GST)], disulfide isomerases [disulfide bond A (DsbA) and disulfide bond C (DsbC)], and periplasm-localizing sequence tags [PelB leader sequence (PelB) and MalE with a signal sequence (MBP)], with several constructs serving in multiple capacities (Table S3).[11,12,20−22] Periplasmic and cytoplasmic expression constructs of MBP were designed to use the T7 expression system present in the other expression systems to provide a direct comparison (Table S4). Three *E. coli* strains were tested, including the workhorse expression strain BL21(DE3), a mutant with dual glutathione oxidoreductase/thioredoxin B deletions ($\Delta gor/\Delta trxB$), and an additional constitutively expressed cytoplasmic chaperone DsbC ($\Delta gor/\Delta trxB/DsbC*$) to further enhance disulfide oxidation (Materials and Methods).[23,24]

Analysis of LC−MS samples of cleaved toxins shows product profiles that vary widely depending on the expression strain and tag (Figure 2A,B). The observed expression yields also displayed a wide range of values, indicating that both the host and fusion tag affect the total amount of expressed protein, proteolysis, and the oxidation level (Figures 2C, S1).

Interestingly, tags with periplasmic signal sequences (PelB and MBP) did not produce sufficient quantities of oxidized DRV, while thioredoxin (Trx) appeared to improve disulfide formation in all cases (Figure 2A).[25,26] The mechanism for Trx influence over cytosolic oxidization of cysteine thiols is unclear and somewhat at odds with the thioredoxin pathway's ascribed biochemical role.[20,27] However, there are a number of reports indicating a role in improving cytosol disulfide formation, where Trx overexpression above typical endogenous concentrations is hypothesized to promote oxidation and aid in disulfide bond formation rather than reduction.[25,26,28] Based on this screen, the Trx tag was selected as the fusion partner for a variety of features: it acts as a solubility enhancer, minimizes proteolysis, and enhances disulfide bond formation under overexpression. Taken together, these results indicate that both the fusion protein and the cytoplasmic chemical environment they create can promote intracellular DRV folding and oxidation.

Among *E. coli* strains, higher levels of oxidation tended to correlate with glutathione oxidoreductase/thioredoxin B knockouts. In general, the reference strain BL21(DE3) produced the most reduced peptide, while both mutant strains produced greater ratios of oxidized peptide. However, when considering total protein production (Figure 2C), the concentration of soluble protein was greater for the strain constitutively producing DsbC (Table S5), which may be attributed to its role in disulfide isomerization. Maximizing total soluble protein and product oxidation, the optimal expression host/fusion tag was ($\Delta gor/\Delta trxB/DsbC*$) with a Trx fusion.

Disulfide formation in *E. coli* expression hosts is natively achieved through fusion to a signal sequence, which directs folding in the oxidizing periplasm; however, recombinant periplasmic production typically produces significantly lower yields than the cytoplasmic expression.[29] Alternatively, mutant strains that lack both glutathione oxidoreductase and thioredoxin B ($\Delta gor/\Delta trxB$) have been shown to promote disulfide oxidation in the cytoplasm.[28] Interestingly, our comparison showed a synergistic effect with the cytoplasm reductase deletions in conjunction with the overexpression of Trx fusion, suggesting that implementation of both of these parameters may be key for high recovery of fully oxidized DRVs, which has not been previously demonstrated. While much about the native biosynthesis of DRVs in their animal hosts remains enigmatic (e.g., disulfide isomerase/chaperone involvement in maturation), synthetic efforts to produce various disulfide-locked peptides have demonstrated the feasibility of folding through disulfide formation in an undirected chemical environment. Examples of peptides containing the inhibitory cysteine knot (ICK) folding in a spontaneous fashion in an oxidizing buffer in the absence of a signal sequence or additional enzymes suggest that backbone conformation is, at least, partially induced by the primary amino acid sequence and can be achieved chemically, analogous to heterologous expression in an oxidizing cytoplasm.[30,31] We thus sought to characterize oxidizing cytoplasmic expression for DRVs more extensively by analyzing the solution structure of additional unrelated sequences.

In Vivo Oxidation Generates Native Knotted Peptide Topologies. Using identical methods of expression and purification, we produced three DRV sequences that originate in diverse organisms (Figure 1, Table S1, and Figure S2). LC−
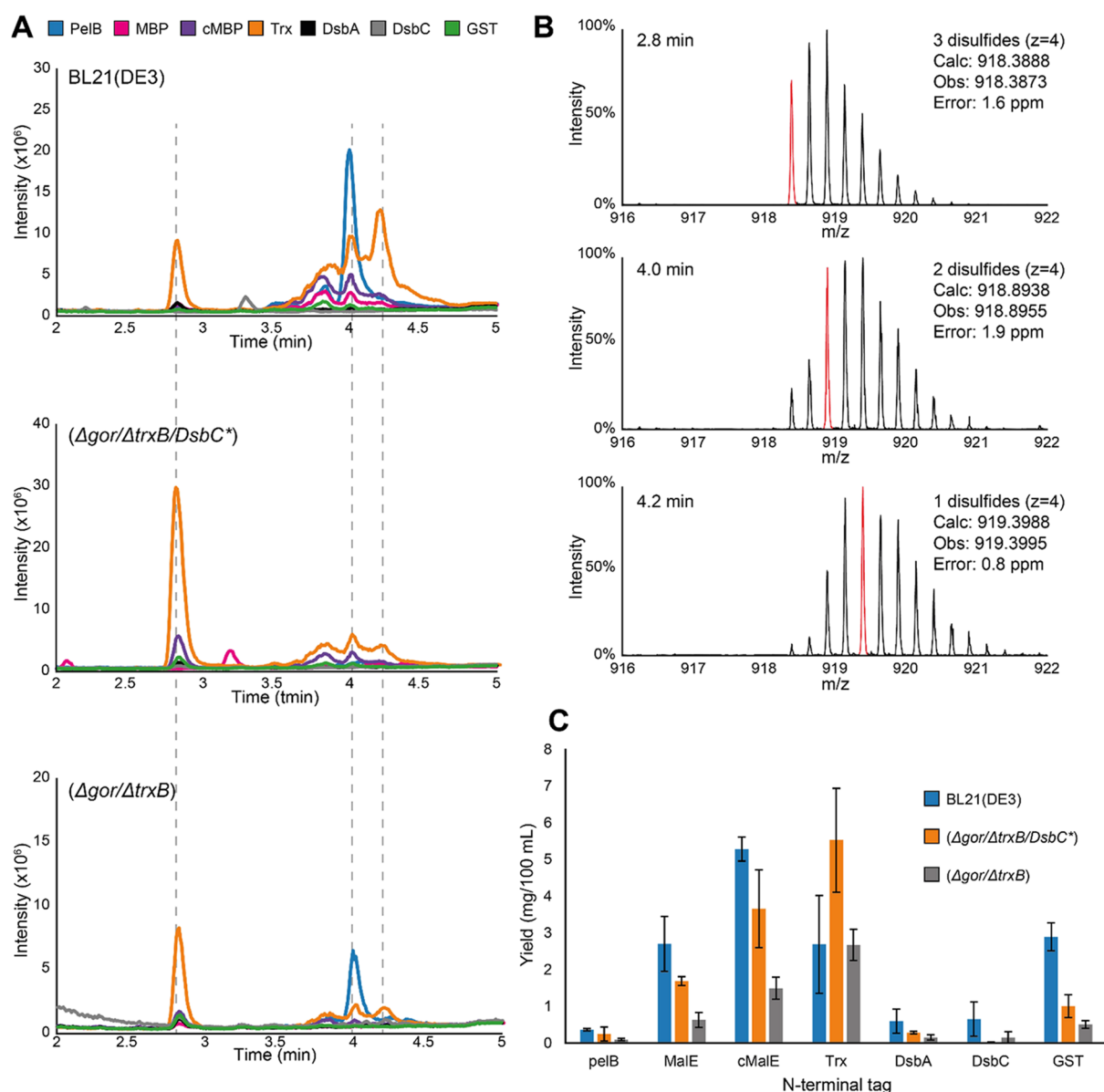
Figure 2. Expression screening of DRV Ptu1. (A) Seven fusion partner tags were expressed in three *E. coli* expression strains, purified by IMAC, cleaved by TEV protease and analyzed by LC−MS. The correct topology eluted at 2.8 min, with major side products at 4.0 and 4.2 min denoted. (B) Corresponding mass spectra of $z = 4$ charge state of Ptu1 at key retention times, indicating the presence of fully and partially oxidized products. Monoisotopic masses (red) for major products shown with calculated and observed masses. (C) Comparison of purified protein yields from the expression screen. Values are averages of three biological replicates; error bars are standard error of mean.

MS analysis of TEV-cleaved peptides indicates that Ptu1 and HWTX-IV produce one major product isomer, while the expressed MVIIA sequence was found to be a mixture of >3 fully oxidized isomers (Figures S3 and S4). We suspect that the mutant expression host was rapidly promoting disulfide formation and prematurely oxidizing incorrect disulfide bonds/conformations. To address this issue, MVIIA was refolded by incubation in a glutathione redox buffer. After chemical refolding, the MVIIA isomer mixture interconverted into a single peak (Figure S4). Chemical refolding in such an undirected fashion requires that the desired topological isomer be the spontaneously folded conformation. While this technique is frequently utilized, it is unclear how often it is applicable, as there likely exist biologically active topologies and conformations that are not most thermodynamically stable and thus would not be obtained by undirected refolding. For

the tested sequences in this study, redox refolding was able to correct misfolded structures to the desired form for MVIIA, suggesting that, generalized for other sequences, a "proof-reading" step can be introduced after expression if evidence of misfolding is present, analogous to the chemical folding process employed for synthetic ziconotide (Prialt),[32] although this must be evaluated individually for unique sequences.

To confirm the structures of the expressed DRVs, purified toxins were analyzed by NMR to compare the previously reported compounds that were isolated from the native producing organisms.[33−35] Due to the highly constrained nature of disulfide-knotted DRVs, under identical sample conditions (temperature and pH), chemical shift values of expressed DRVs would closely match reported shifts for native-sourced compounds, particularly for the backbone portions of the peptides. For our first analyzed compound, Ptu1, the

difference in individual shifts was <0.1 ppm (Figure 3), indicating a strong topological match and validating that the
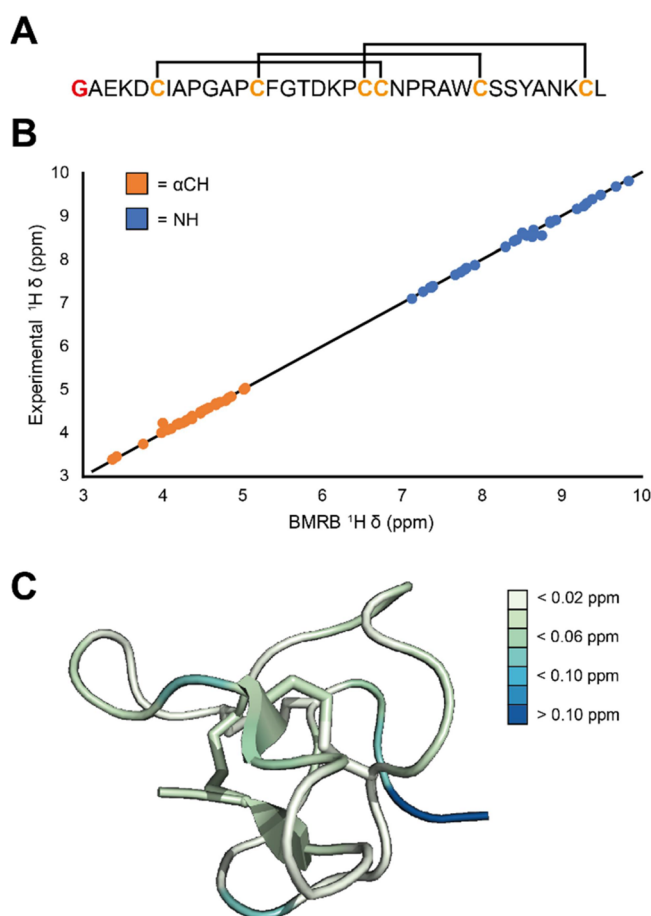

Figure 3. Topology structural characterization of Ptu1. (A) Sequence for Ptu1 with N-terminal Gly from TEV cleavage (red) and bridging Cys residues (orange). (B) Comparison of backbone 1H NH (blue) and αCH (orange) in bacterial recombinant Ptu1 to the reported structure (PDB 1I26 and BMRB 5039). (C) Mapping average $[(\Delta\delta\alpha CH + \Delta\delta NH)/2]$ shift differences (ppm) to solution structure showing regions of low variance (lighter) to high variance (darker).

biosynthetically produced compound matches the native version. The regions of highest variance localized to the linear N-terminus and distal regions of some loops (Figure 3C). Other loops showed extremely low NMR shift variance, suggesting that a certain degree of structural rigidity is endowed by the loop sequence itself and is not only a proximal effect of the disulfides. A similar fingerprinting analysis for the other recombinant DRVs revealed that these sequences also conformed to their respective reported structures (Figures S5−S10 and Tables S6−S8).

To test the applicability for functional studies of DRVs, we applied this workflow to the sea anemone toxin ATX-II from *Anemonia sulcata*. We chose this compound because of its bioactivity as a known modulator of voltage-gated sodium channels (Na$_V$ subtype 1.1), activating current flow through delay of channel inactivation (Table S1).[36−38] We reasoned that this unique mode of action would (i) be readily identifiable through a diagnostic electrophysiology experiment and (ii) present a biological effect that would only result from a correctly folded structure (unlike a more general inhibition mechanism, such as pore blocking). Expression of ATX-II

followed procedures used for the other DRVs reported here and resulted in a successful expression of a full-length, oxidized peptide (Figure S11). We hypothesized that the most time-consuming steps of purification and structural analysis could be eliminated in cases where MS analysis indicated robust expression, such as ATX-II; after tag removal and solid-phase extraction (Materials and Methods, Figure S2), the partially purified toxin was assessed for its ability to modulate channel activity of a Na$_V$1.1-expressing cell line via a patch clamp experiment. Recombinantly expressed, semi-purified ATX-II displayed a dose-dependent increase in current relative to DRV concentration, similar to its previously reported EC$_{50}$ (Figure 4A,B).[36] Importantly, increases in late current values after
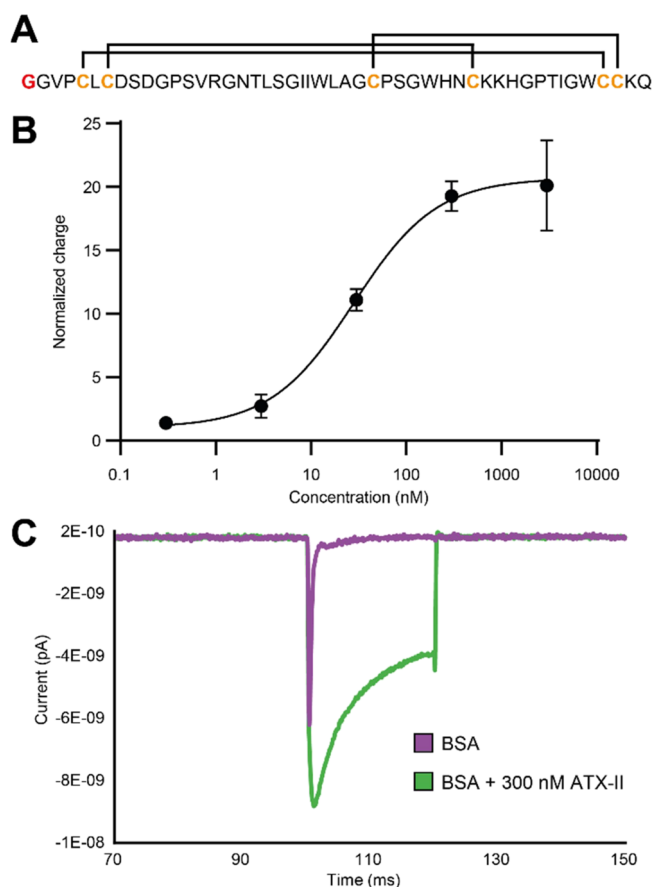

Figure 4. Bioactivity confirmation of knotted ATX-II. (A) Sequence for ATX-II with N-terminal Gly from TEV cleavage (red) and bridging Cys residues (orange). (B) Recombinant ATX-II was tested for its ability to activate NaV1.1 channels. Dose-dependent current activation was seen with a calculated EC$_{50}$ 28 nM. (C) Representative current trace showing delay of inactivation by ATX-II in the late current region. Currents were elicited by 20 ms depolarization from −100 to −10 mV at 0.45 Hz.

channel opening suggest that the biosynthesized compound's mode of action is consistent with the distinctive delay of inactivation, resulting in the hallmark tailing current (Figure 4C). In contrast to previous recombinant production of ATX-II, the correctly folded topology was obtained here directly from in-cell oxidation, eliminating a time-consuming chemical folding.[39] These results suggest that this expression method-ology could be used to rapidly synthesize functional DRVs for proof-of-concept experiments where rapid testing or screening toxin libraries is prioritized.

Knotted Disulfide Structure Plays a Key Role in Vivo Stability. With a verified method for production of the folded knotted peptides, we investigated DRV properties, including PK properties that inform drug properties and structural features that inform fundamental aspects of biosynthesis. Various DRV scaffolds have emerged as candidates for drug development, both as modulators of their natural targets as toxins and as scaffolds that provide targeting domains for tracers or chemical warheads.[40,41] Posttranslational modification of peptides, such as macrocyclization and heterocyclization, is thought to be used in nature to increase rigidity and reduce degradation in biological contexts.[42] Specifically, interlocking disulfide topologies seen in DRVs have been suggested to increase residence time in vivo.[6] To characterize the effects of the interlocking disulfides present on the common ICK motif, Ptu1 was analyzed for its stability in plasma in vitro. Samples of Ptu1 that were either fully folded/oxidized or linear/reduced were diluted into a matrix of mouse plasma and sample up to 24 h. Extensive degradation was apparent for the linear form, as it was below the limit of detection in the first time point sampled (Figure 5A). By contrast, the folded form of Ptu1 was stable out to the longest time point tested at a consistent concentration, suggesting no detectable amount of degradation in plasma. As character-

ization of the venom proteome ("venomics") continues to reveal the diversity of knotted peptides, this result supports the assertion that this post translational modification (PTM) benefits these molecules in their delivery to extracellular targets.[3,32,43]

We sought to evaluate the folded form of Ptu1 in an in vivo system to understand whether the plasma PK properties translate to in vivo characteristics. Intravenous 1 mg/kg administration in rat models showed a $t_{1/2}$ of 25 min, with a low clearance (CL = 7 mL·min^{-1}·kg^{-1}) (Figure 5B), atypical for a peptide of this size. In light of its low steady-state volume of distribution (V_{SS} = 0.2 L·kg^{-1}), we hypothesize that protein binding is not responsible for the characteristic low rate of CL. Taken in conjunction with the plasma stability, we expect renal CL to be the primary mode of elimination of knotted peptides, while linear forms are susceptible to endogenous proteases present in circulation. Based on the simultaneously low CL and V_{SS} values, it appears that evasion of proteolytic mechanisms is key, particularly for DRV compounds interacting with an extracellular target. These data suggest the knotted disulfides that are present on many molecules from nature play a role in stability by reducing systemic CL and is consistent with its wide occurrence in venom toxins, which must remain stable after envenomation until target engagement. Incorporation of a knotted topology into known bioactive peptide epitopes may present an optimization strategy by increasing $t_{1/2}$ and evading intrinsic CL mechanisms that limit peptide therapeutics.

Backbone Organization Mediates Concomitant Disulfide Formation. Despite development of DRV scaffolds into therapeutics and efforts to control engineered disulfide topologies into new sequences, little is known about the folding process of biologically abundant, naturally occurring knotted peptides.[44] Previous studies have investigated the chemical folding process of DRVs in an endpoint-based chromatographic assay.[45−47] However, real-time monitoring of structure development during folding would provide insights into backbone organization without the need for bond formation, providing information on conformational states, rather than disulfide intermediates. Indeed, for folding processes that are not disulfide-driven, spectroscopic analysis of backbone conformation is key to understanding topology pathways. To study real-time monitoring of peptide folding, we performed isotope incorporation to generate ^{15}N-labeled peptides for heteronuclear single quantum coherence (HSQC) NMR. ^{15}N-labeled versions of Ptu1 were biosynthetically produced via ^{15}NH$_4$Cl feeding, and isotope incorporation was confirmed by MS (Materials and Methods, Figure S12).[48] ^{15}N-Ptu1 was linearized by reduction in glutathione/tris(2-carboxyethyl)phosphine (TCEP) buffer; refolding was then initiated using oxidized glutathione disulfide (GSSG) and monitored using ^{1}H-^{15}N-HSQC NMR.

In the initial reduced state, ^{15}N-Ptu1's HSQC spectrum shows heavily overlapping amide signals between 7.5 and 8.5 ppm, consistent with an unfolded, disordered structure. Upon addition of the oxidizing initiation reagent, refolding occurs, allowing for subsequent acquisitions to function as snapshots of the folding process. During refolding, signals in the amide region (6.5−10 ppm) become significantly more dispersed (Figure 6A), indicating movement toward an ordered topology. Intensities of backbone amide peaks over time were analyzed to plot topology organization completion. As evident from the saturating curve of peak intensities, major folding is completed within 36 h (Figure 6, Table S9, and
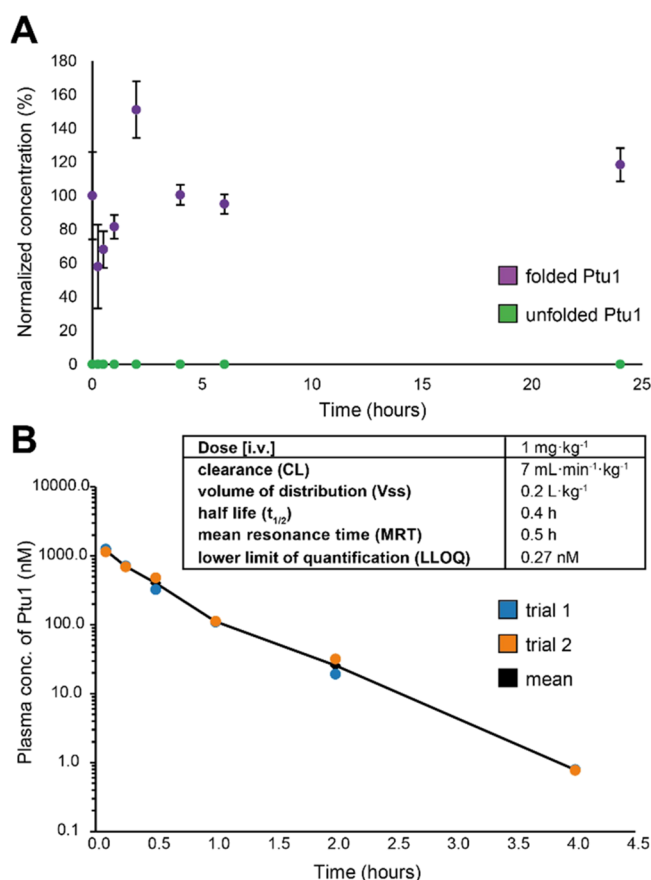
Figure 5. Pharmacokinetic properties of Ptu1. (A) Plasma stability tests of Ptu1 were performed with LC−MS time-course sampling of folded (purple) and unfolded (green) samples. (B) Ptu1 was dosed intravenously in two Sprague−Dawley rats at 1 mg/kg, and serum sampling was used to determine stability in vivo. Calculated PK parameters are shown in the inset. Two biological replicates (blue and orange) and mean (black) are shown.

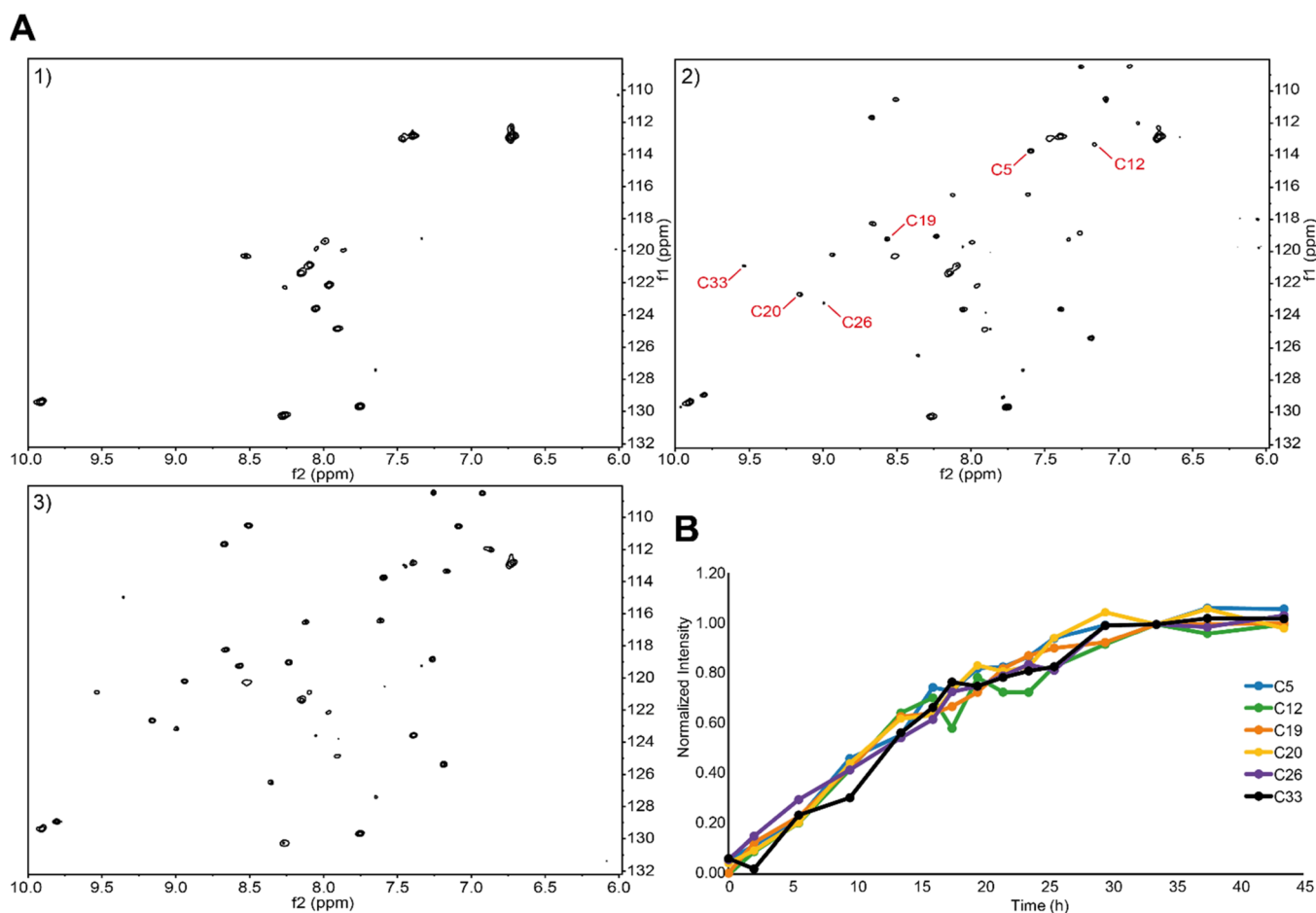| Dose [i.v.]	1 mg·kg^{-1}
clearance (CL)	7 mL·min^{-1}·kg^{-1}
volume of distribution (Vss)	0.2 L·kg^{-1}
half life ($t_{1/2}$)	0.4 h
mean resonance time (MRT)	0.5 h
lower limit of quantification (LLOQ)	0.27 nM

Figure 6. Time-course HSQC of Ptu1 refolding. (A) Starting from a reduced, linear form (1), folding was initiated by the addition of GSSG and monitored with HSQC acquisitions. Shown are snapshots at approximately 50% (2) and 100% (3) folded with Cys residues identified. (B) Disulfide preorganization—Cys residue peak intensities normalized against final intensities plotted to indicate backbone organization.

Figures S13−S16), although some minor backbone motion continues afterward.

Estimated rates of folding were determined for individual residues by fitting normalized signal intensity to a limited exponential function. Interestingly, all backbone signals showed nearly equivalent rates of folding based on fit rate constants (Figures 6B and S17). Initially, we expected sequential disulfide oxidation to drive formation of the knotted topology; instead, rate data are highly consistent with a concerted, simultaneous folding (Figure S17), suggesting backbone arrangement, rather than disulfide formation driving folding. These findings provide evidence that the primary sequence of the DRV itself plays a key role in its conformational arrangement and that disulfide formation occurs after this preorganization. Together, these data may suggest that unbiased, randomized libraries based on known ICK archetypes (i) may not necessarily fold effectively as sequence changes could perturb this preorgnization encoded in the primary sequence for folding that is not disulfide-driven and (ii) may consequently lack PK benefits the topology endows.

In general, only positive folding events were observed for assigned peaks, suggesting that the knotted fold proceeded only through a "productive" folding pathway and did not appreciably sample off-pathway conformations. This is corroborated by the distinct lack of transient intermediate peaks, which form and then fade. This type of productive folding pathway has been noted for certain knotted sequences, although they are not universal, with examples of "off-pathway" intermediates.[45,49] We expect that the assay described here can be applied to the diversity of folding patterns that emerge from the wealth of DRV sequences present in nature, as well as toward the de novo design of new-to-nature knottin sequences.

■ CONCLUSIONS

The synthesis of knotted peptides faces intrinsic challenges due to both the topological character endowed by the interlocking disulfide bonds and their large size. To better understand features that influence bacterial recombinant production, we screened expression parameters and characterized several peptides by NMR to validate the correct folding topology and chemical refolding as a means to promote correct isomer formation. Additionally, a DRV was produced without preparatory chromatography and structural fingerprinting, utilizing bioactivity-based characterization relevant for DRVs with established modes of action or multiplexed screening efforts (e.g., a codon library of analogues) in which rapid analysis is prioritized or where a specific topology is not required. With our production methods, we sought to understand the properties of DRVs that might influence their translation to drug development and production. We found that the knotted, globular nature of DRVs contributes to its stability, particularly in a serum environment, and that in vivo

CL was surprisingly slow, resulting in a proposed mechanism of CL. These properties likely contribute to the ubiquity of knotted DRVs in nature as a way to avoid typical liabilities associated with peptide scaffolds (e.g., short half-life and fast CL). Lastly, we aimed to further understand the folding process that DRVs adopt during maturation. Given a proper redox environment (intracellularly, as for recombinant microbial production, or chemically, as for synthetic folding), there are many examples of knotted peptides folding in the absence of chaperone systems. To study this phenomenon, we developed an NMR-based assay to monitor backbone organization in solution during folding. This approach allowed for an unprecedented level of resolution, giving direct evidence that primary sequence preorders the backbone for folding and can aid in investigating the folding of other topologies and sequences.

■ MATERIALS AND METHODS

General Materials and Methods. Reagents used for molecular biology experiments were purchased from New England Biolabs (NEB, Ipswich, MA). Other chemicals were purchased from Sigma-Aldrich (St. Louis, MO) or Thermo Fisher Scientific (Waltham, MA), unless stated otherwise. *Escherichia coli* DH5α, BL21(DE3), and Shuffle T7 Express ($\Delta gor/\Delta trxB/DsbC^*$) strains were purchased from NEB, and Origami2 strain ($\Delta gor/\Delta trxB$) was purchased from Novagen/EMD-Millipore. Plasmid vectors were obtained from Novagen/EMD-Millipore for pET expression vectors. Media was purchased from Teknova (Hollister, Ca). LC−MS analyses were performed using a TripleTOF 6600 Quadrupole Time-Of-Flight (SCIEX) equipped with an ACQUITY ultra-performance liquid chromatography (UPLC) system (Waters). Plasma stability assay and in vivo PK assay were performed on a Thermo Q Exactive HF-X mass spectrometer coupled to a Thermo Vanquish UPLC system.

Molecular Biology Techniques. Oligonucleotides and *E. coli* codon-optimized genes were purchased from Integrated DNA Technologies Inc. (Coralville, IA). Cloning was performed using Gibson assembly with an NEBuilder HiFi Assembly cloning kit according to manufacturer's specifications. The primers for constructs are listed in Table S2. Constructs were verified by Sanger sequencing using the appropriate forward primer and the T7 reverse primer at Genewiz (Cambridge, MA).

Expression Screening Cell Lines and Fusion Tags. *E. coli* BL21(DE3) chemically competent cells (*fhuA2 [lon] ompT gal (λ DE3) [dcm] ΔhsdS λ DE3 = λ sBamHIo ΔEcoRI-B int::(lacI::PlacUV5::T7 gene1) i21 Δnin5*), Shuffle T7 Express competent cells (*fhuA2 lacZ::T7 gene1 [lon] ompT ahpC gal λatt::pNEB3-r1-cDsbC (SpecR, lacIq) ΔtrxB sulA11 R(mcr-73::miniTn10--TetS)2 [dcm] R(zgb-210::Tn10 --TetS) endA1 Δgor Δ(mcrC-mrr)114::IS10*), and Origami 2(DE3) competent cells (*Δ(ara-leu)7697 ΔlacX74 ΔphoA PvuII phoR araD139 ahpC galE galK rpsL F′[lac + lacIq pro] (DE3) gor522::Tn10 trxB (StrR, TetR)*) were transformed according to manufacturer instructions with 100 ng of pET26-PelB, pET28-MBP, pET28-cMBP, pET32-Trx, pET39-DsbA, pET40-DsbC, or pET42-GST constructs and selected with either 50 μg/mL of kanamycin or 100 μg/mL of carbenicillin and 10 μg/mL of tetracycline for Origami 2(DE3) samples. Constructs were designed to express Ptu1 as a C-terminal fusion immediately downstream of an inserted TEV protease

site and internal His$_6$ tag or as C-terminal fusions to MBP immediately downstream of a TEV site.

Single colonies were used to inoculate 10 mL of Lysogeny Broth (LB) containing a selection marker and grown at 30 °C for 20 h. This culture was used to inoculate 100 mL of LB containing the appropriate selection marker and grown to an optical density OD600 of 0.6. Protein expression was induced with the addition of 400 μM isopropyl β-D-1-thiogalactopyranoside (IPTG) for 16 h at 16 °C. Cells were harvested by centrifugation at 4700 rpm for 20 min, washed with phosphate-buffered saline (PBS), and centrifuged at 4700 rpm for 20 min. Cell pellets were stored at −80 °C until purification.

Cell pellets were resuspended in 30 mL of MBP lysis buffer [50 mM Tris−HCl pH 7.5, 500 mM NaCl, 0.1% Triton X-100, and 2.5% glycerol (v/v)] for MBP constructs or NTA lysis buffer for others [50 mM Tris−HCl pH 8.0, 300 mM NaCl, 15 mM imidazole, 0.1% Triton X-100, 2.5% glycerol (v/v)] containing 4 mg/mL of lysozyme and 100 μL of Protease Inhibitor Cocktail Set III (EDTA-free, MilliporeSigma). Cells were homogenized by sonication (3 × 30 s on ice with 10 min equilibration periods at 4 °C with rocking) using a Q500 sonicator (500 W) at 60% power (Qsonica, Newton, CT). Insoluble cell debris was removed by centrifugation at 10,000 rpm for 60 min at 4 °C. The supernatant was then loaded onto 1 mL of pre-equilibrated amylose or Ni-NTA resin (NEB, Thermo Fisher Scientific). Columns were washed with 30 mL of the appropriate lysis buffer and 30 mL of MBP wash buffer [50 mM Tris−HCl pH 7.5, 300 mM NaCl, 2.5% glycerol (v/v)] or 90 mL of NTA wash buffer [50 mM Tris−HCl pH 8.0, 500 mM NaCl, 20 mM imidazole, 2.5% glycerol (v/v)]. Proteins were eluted using 30 mL of MBP elution buffer [50 mM Tris−HCl pH 7.5, 300 mM NaCl, 10 mM maltose, 2.5% glycerol (v/v)] or NTA elution buffer [50 mM Tris−HCl pH 8.0, 500 mM NaCl, 250 mM imidazole, 2.5% glycerol (v/v)]. The elution fraction was concentrated and buffer-exchanged with storage buffer [50 mM HEPES pH 7.3, 300 mM NaCl, 2.5% glycerol (v/v)] using a 3 kDa MWCO Amicon Ultra centrifugal filter (Millipore) for PelB constructs or 10 kDa MWCO for all others. Purified fusion proteins were stored at −80 °C. Protein concentrations were determined using 280 nm absorbance (extinction coefficients were calculated using the ExPASy ProtParam tool; http://web.expasy.org/protparam/).

1 L Scale Fusion Protein Expression and Purification. *E. coli* Shuffle T7 Express cells were transformed with 100 ng of plasmid for toxin expression. Cells were grown for 24 h on LB agar plates containing either 50 μg/mL of kanamycin or 100 μg/mL of carbenicillin at 30 °C. Single colonies were used to inoculate 10 mL of LB containing a selection marker and grown at 30 °C for 20 h. This culture was used to inoculate 1 L of LB containing the appropriate selection marker and grown to an optical density OD600 of 0.6. Protein expression was induced with the addition of 400 μM IPTG for 16 h at 16 °C. Cells were harvested by centrifugation at 4700 rpm for 20 min, washed with PBS, and centrifuged at 4700 rpm for 20 min. Cell pellets were stored at −80 °C until purification.

Cell pellets were resuspended in 30 mL of lysis buffer [50 mM Tris−HCl pH 8.0, 300 mM NaCl, 15 mM imidazole, 0.1% Triton X-100, 2.5% glycerol (v/v)] containing 4 mg/mL of lysozyme and 100 μL of Protease Inhibitor Cocktail Set III (EDTA-free, MilliporeSigma). Cells were homogenized by sonication (3 × 30 s on ice with 10 min equilibration periods at 4 °C with rocking) using a Q500 sonicator (500 W) at 60%

power (Qsonica, Newton, CT). Insoluble cell debris was removed by centrifugation at 10,000 rpm for 60 min at 4 °C. The supernatant was then loaded onto 3 mL of pre-equilibrated Ni-NTA resin (Thermo Fisher Scientific). The column was washed with 30 mL of lysis buffer followed by 90 mL of wash buffer [50 mM Tris−HCl pH 8.0, 500 mM NaCl, 20 mM imidazole, and 2.5% glycerol (v/v)]. The His-tagged proteins were eluted using 30 mL of elution buffer [50 mM Tris−HCl pH 8.0, 500 mM NaCl, 250 mM imidazole, 2.5% glycerol (v/v)]. The elution fraction was concentrated and buffer-exchanged with storage buffer [50 mM HEPES pH 7.3, 300 mM NaCl, and 2.5% glycerol (v/v)] using a 10 kDa MWCO Amicon Ultra centrifugal filter (Millipore). Purified toxin fusion proteins were stored at −80 °C. Protein concentrations were assayed using both 280 nm absorbance (extinction coefficients were calculated using the ExPASy ProtParam tool; http://web.expasy.org/protparam/) and Bradford colorimetric assay using bovine serum albumin (BSA) as a standard (Thermo Fisher Scientific).

TEV Protease Toxin Tag Cleavage. TEV protease was added to Trx-tagged toxins in 20 mol % in reaction buffer (50 mM Tris−HCl pH 7.5, 125 mM NaCl, and 20 mM MgCl$_2$ 7· H$_2$O) and reacted at 25 °C for 6−20 h. Protease and tag were removed from reaction mixtures by flowing over 2 mL of equilibrated Ni-NTA resin. The flow through was collected, and any additional peptide was washed with Ni-NTA buffer (50 mM Tris−HCl pH 8.0, 150 mM NaCl). Samples were desalted using a C18 HyperSep SPE cartridge (Thermo Fisher Scientific, 1 g bed weight), which was equilibrated with 10 mL of MeCN +0.1% formic acid (FA), 10 mL of 50% MeCN aq. + 0.1% FA, and 20 mL of 5% MeCN aq. + 0.1% FA. Loaded samples were washed with 10 mL of 5% MeCN +0.1% FA and eluted with 10 mL of 80% MeCN aq. + 0.1% FA and dried under reduced pressure.

HPLC Purification of Toxins. Toxins were purified using a Waters HPLC equipped with Waters 2545 binary gradient module pumps, a Waters 2767 sample manager/fraction collector, Waters XSelect CSH Prep C18 preparatory column (19 × 150 mm), and a Waters Acquity QDa electrospray ionization (ESI) single-quadrupole mass analyzer. Samples were dissolved in a minimal amount of 50% MeCN aq. + 0.1% FA and injected with a gradient mobile phase of water/MeCN +0.1% trifluoroacetic acid (TFA, v/v) from 5−15% organic over 10 min at a flow rate of 30 mL/min. Elution was monitored by absorbance at 280 nm and by mass spectrometry. Fractions containing the toxins were flash-frozen in isopropanol/dry ice bath and lyophilized to dryness.

To remove TFA counterions, samples were subjected to ion exchange to scavenge trifluoroacetate. Mini SiliaPrep SPE carbonate cartridges (Silicycle) were washed with 10 mL of water and then 20 mL of 0.1% FA aq. A toxin sample was dissolved in 10 mL of 0.1% FA aq. and then passed through the cartridge by a syringe, and the flow through was collected. An additional 10 mL of 0.1% FA aq. was used to wash the cartridge and pooled with the flow through and then lyophilized.

Mass Spectrometric Characterization of Toxins. Tagged toxins (100 μg) were TEV-cleaved in a final volume of 100 μL, and 10 μL was injected into a Waters Acquity UPLC system equipped with an ACE Excel 2 C18-Amide column (50 × 2.1 mm id, 2 μm particle size) and Sciex TripleTOF 6600 ESI quadropole time-of-flight mass analyzer. TEV cleavage reactions or purified toxins were diluted to 0.1 mg/mL, and 10 μL was injected with a gradient mobile phase of water/MeCN +0.1% FA over 6 min from 0−30% MeCN at a flow rate of 0.6 mL/min.

Chemical Refolding of Toxins. HPLC-purified toxins that were determined to be a mixture of multiple isomers were refolded by dissolving the compounds in a glutathione-based refolding buffer. Toxins were dissolved in a buffer containing 500 mM NH$_4$OAc (pH 7.9), 1 mM glutathione, and 0.1 mM GSSG. Reactions were incubated at 4 °C for up to 72 h. Refolding was monitored by UPLC.

Stable Isotope Labeling of Recombinant Toxins. Isotopically labeled toxins were produced via a modified expression workflow utilizing induction in minimal media containing ^{15}N NH$_4$Cl (≥98% atom) in a procedure adapted from the work of Marley et al.[48] Briefly, *E. coli* Shuffle T7 Express cells were transformed with plasmid for toxin expression. Cells were grown for 24 h on LB agar plates containing either 50 μg/mL of kanamycin or 100 μg/mL of carbenicillin at 30 °C. Single colonies were used to inoculate 10 mL of LB containing a selection marker and grown at 30 °C for 20 h. This culture was used to inoculate 1 L of LB containing the appropriate selection marker and grown to an optical density OD600 of 0.6. Cultures were centrifuged at 4700 rpm for 30 min and suspended in 250 mL of M9 minimal media +2% glucose (Teknova) + 0.1% ^{15}NH$_4$Cl (Sigma) and incubated at 30 °C for 1 h. Cells were again harvested by centrifugation at 4700 rpm for 30 min and suspended in 250 mL of fresh M9 minimal media +2% glucose +0.1% ^{15}NH$_4$Cl and induced with 800 μM IPTG at 16 °C for 16 h. The final OD$_{600}$ at harvest was 1.0, and cell pellets were collected and frozen at −80 °C until purification.

NMR Characterization of Toxins. HPLC-purified toxins were made into 3 mM solutions in 90% H$_2$O/10% D$_2$O (Cambridge Isotope Labs, >99.8% atom). Spectra were recorded on a Bruker Avance 600 MHz NMR spectrometer. NMR spectra were recorded on a 600 MHz Bruker AVANCE III HD instrument equipped with a QCI-F cryoprobe (Bruker Biospin, Billerica, MA, USA). Data were collected at different temperatures to match assignments published previously. Standard Bruker pulse sequences were used for each of the following experiments: ^{1}H-NMR, ^{1}H-^{1}H correlation spectroscopy (COSY), ^{1}H-^{1}H total correlation spectroscopy (TOCSY) (80 ms mixing time), and ^{1}H-^{1}H nuclear Overhauser effect spectroscopy (NOESY) (400 ms mixing time). Solvent suppression by presaturation was employed for ^{1}H, ^{1}H-^{1}H NOESY, and ^{1}H-^{1}H TOCSY. Spectra were recorded and processed with Topspin 3.5.

Automated Patch Clamp Assay of Toxins. hNav1.1-HEK293 recombinant cell lines (Millipore, MA) were grown in a T175 cm^2 flask using D-MEM/F-12 media (Invitrogen) supplemented with 10% fetal bovine serum (Invitrogen), 1% nonessential AA (Invitrogen), and 400 μg/mL of geneticin (Invitrogen). When the cells reached ~60−70% confluence, they were washed with 5 mL of PBS at 37 °C, followed by detachment using Detachin (Genlantis, CA) and suspended at a density of 2 million cells/mL in IMDM (Invitrogen), supplemented with 10% dialyzed fetal bovine serum (Invitrogen), 1% HT supplement (Invitrogen), and 1% nonessential AA (Invitrogen). The cells were left on a rotating shaker at room temperature prior to use (<1 h).

Internal solution contained 120 mM CsF, 20 mM NaCl, 5 mM HEPES, and 5 mM EGTA, and pH of the solution was adjusted to 7.2 with CsOH. The osmolarity was verified as

~300 mOsm. The solution was filtered with a 0.2 μm filter before use. External solution contained 60 mM NaCl, 1 mM CaCl$_2$, 2 mM MgCl$_2$, 84 mM TEA-Cl, and 10 mM HEPES, and pH of the solution was adjusted to 7.4 using NaOH. The osmolarity was verified as ~293. The solution was filtered with a 0.2 μm filter before use. External solution supplemented with 10% BSA was used as reference solution. ATX-II was dissolved into stock solutions of 10 mM in reverse-ionized distilled water, and concentration was estimated using the calculated extinction coefficient at 280 nm (https://web.expasy.org/protparam/). For potentiation experiments, currents were elicited via step from bath solution to solution supplemented with ATX-II serially diluted to the required solution in reference solution.

Resting membrane potential was fixed at −100 mV, and peak current was recorded by ramping the potential to −10 mV. The area under the curve (AUC) was integrated to calculate the total amount of charge passing through the channel. Charge from all cells were normalized to the charge when reference solution was applied. All traces were recorded and analyzed using the Sophion Analyzer (Sophion Bioscience, Denmark).

Plasma Stability Assay. A total of 100 and 1000 nM solutions of the compound were prepared in mouse plasma with a final volume of 500 μL and incubated at 37 °C in a water bath with a shaker at 500 rpm. A total of 20 μL was transferred to 150 μL of methanol on ice for protein precipitation at 0, 0.25, 0.5, 1, 2, 4, 6, and 24 h. The samples were vortexed and centrifuged at 4000 rpm for 15 min at 4 °C. A 125 μL aliquot of supernatant was transferred to a 96-well plate, and 100 μL of water was added to each well and vortexed for LC−MS/MS analysis. A total of 10 μL was injected into a Thermo Q Exactive HF-X mass spectrometer coupled to a Thermo Vanquish UPLC system. Compounds were analyzed using a Waters Protein BEH C4 analytical column (1.7 μm particle size; 50 × 2.1 mm id). The mobile phase consisted of solvent A (0.1% FA aq.) and solvent B (0.1% FA in MeCN). A linear gradient was programmed from 5 to 95% B from 0.5 to 3.5 min, with a flow rate of 500 μL/min and a total method run time of 4.5 min. Samples were detected using full scan (Resolution: 120,000; AGC Target: 3 × 10^6; Maximum IT: 200 ms) with a scan range of 400 to 1250 m/z in positive ion mode.

In Vivo PK Assay. All in vivo research was reviewed and approved by the Novartis Institutes of Biomedical Research Institutional Animal Care and Use Committee in accordance with applicable local, state, and federal regulations.

PK studies were conducted in male Sprague−Dawley rats (n = 2). Ptu1 was formulated in solution in PBS to 2.0 mg/mL, and 0.5 mL/kg (1.0 mg/kg dose) of this was dosed intravenously via injection into the jugular vein cannula. Approximately 50 μL of whole blood was collected from each animal via a jugular vein cannula at 5 min, 15 min, 0.5, 1, 2, 4, 7, 24, 30, and 48 h post-dose and transferred to EDTA tubes. Blood samples were centrifuged at 3000 rpm, and the resultant plasma supernatant was transferred to a capped PCR 96-well plate and frozen at −20 °C until subsequent preparation and analysis by HPLC−MS/MS.

PK Bioanalytical Method. A 20 μL volume of blank plasma was used for calibration standards and quality control (QCs). The standards and QCs were prepared by serial dilution into blank plasma from 1 mg/mL standard stock solution in dimethyl sulfoxide: methanol (1:1). A total of 20

μL of plasma was used for the unknown samples. The unknown samples were prepared as a 2× dilution with 10 μL of blank plasma and 10 μL of the sample. These standards, QCs, and unknowns were prepared in the appropriate wells of 96-well assay plates. A total of 150 μL of the ISTD and protein crash solution (100 ng/mL of liraglutide in methanol) was added into all wells. The plate was shaken strongly in a plate shaker for approximately 5 min and then centrifuged at 4000 rpm, 4 °C, for 10 min. A 125 μL aliquot of the supernatant was transferred to a 96-well plate, and 100 μL of water was added to each well and vortexed for LC−MS/MS analysis. A total of 10 μL was injected into a Thermo Q Exactive HF-X mass spectrometer coupled to a Thermo Vanquish UPLC system. Compounds were analyzed using a Waters Protein BEH C4 analytical column (1.7 μm particle size; 50 × 2.1 mm id). The mobile phase consisted of solvent A (0.1% FA aq.) and solvent B (0.1% FA in MeCN). A linear gradient was programmed from 5 to 95% B from 0.5 to 3.5 min, with a flow rate of 500 μL/min and a total method run time of 4.5 min. Samples were detected using Targeted-SIM mode (Resolution: 120,000; AGC Target: 1 × 10^5; Maximum IT: 200 ms) in positive ion mode.

PK Sample Analysis and Calculations. Standard curve solutions of Ptu1 were prepared from 1 mg/mL PBS stock solution serially diluted into blank rat plasma to final concentrations of 10,000 to 0.1 ng/mL. These standard curve samples were prepared for LC/MS/MS like the PK plasma samples below.

PK plasma samples were thawed, and 10 μL aliquots of each sample +10 μL blank plasma (or 20 μL standard curve solution) were transferred to a 96-well deepwell plate and gently shaken for 5 min. A 150 μL aliquot of extraction solution (100% methanol containing 100 ng/mL of liraglutide as internal standard) was added to each well. The plate was covered and mixed for approximately for 5 min on a pulse-vortex mixer. The plate was centrifuged at 4000 rpm for 10 min at 4 °C. A 125 μL volume of the resulting supernatant was transferred into the corresponding well of a clean 1 mL 96-well assay plate and mixed with 100 μL of water. Samples and standard curve samples were analyzed by LC/MS as mentioned above.

PK parameters were derived from plasma concentration values by noncompartmental analysis using Excel. Terminal half-life ($t1/2$) = −0.693/kel, where kel is the slope of the line formed from the times of the last three measured concentrations vs the natural log of the last 3 measured concentrations. The AUC was calculated by the linear trapezoidal rule: AUC = $(C_1 \times t_1)/2 + \sum_{i=1}^{n-1} (t_{i+1} - t_i) \times (C_i + C_{i+1})/2$. The extrapolated AUC (AUC$_{inf}$) = AUC + $C_{last} \times t1/2/0.693$, where C_{last} is the last quantifiable concentration. The area under the moment curve (AUMC) was calculated by the following equation: AUMC = $(C_1 \times t_1^2)/2 + \sum_{i=1}^{n-1} (t_{i+1} - t_i) \times (C_i \times t_i + C_{i+1} \times t_{i+1})/2$. Mean residence time (MRT) was calculated by the following equation: MRT = AUMC/AUC. CL was calculated by the following equation: CL = (Intravenous dose)/AUC$_{inf}$. Volume of distribution (V_{dss}) was calculated by the following equation: V_{dss} = CL × MRT.

NMR Solution Refolding Assay. ^{15}N-labeled Ptu1 were dissolved in 0.2 mL of reducing buffer [10 mM Na$_2$B$_4$O$_7$ pH 7.9, 1 mM glutathione, and 1.5 mM TCEP] and heated at 50 °C for 90 min to yield fully reduced peptide. Refolding was initiated with the addition of 0.1 mM GSSG made as a 10× stock (10 mM Na$_2$B$_4$O$_7$ pH 7.9 and 1 mM GSSG), and ^{1}H-^{15}N

HSQC spectra were taken with 40 min acquisitions with samples held at 238 K during refolding. After assignment of the Ptu1 backbone residues, peak intensities were obtained by calculating peak height at each time point and normalized to final intensity to determine folding completion. Data analysis was performed with GraphPad Prism 8.42.

■ ASSOCIATED CONTENT

Ⓢ Supporting Information

The Supporting Information is available free of charge at https://pubs.acs.org/doi/10.1021/acsomega.1c03707.

> Recombinant expression parameters, purification, refolding, and structural characterization of compounds, including LC−MS and ^{1}H, COSY, TOCSY, and NOESY NMR data, isotopic label incorporation, and HSQC folding assay (PDF)

■ AUTHOR INFORMATION

Corresponding Authors

Tejas P. Pathak − *Global Discovery Chemistry, Novartis Institutes for Biomedical Research, Cambridge, Massachusetts 02139, United States;* ⦿ orcid.org/0000-0003-3858-8770; Email: tejas.pathak@novartis.com

Piro Siuti − *Global Discovery Chemistry, Novartis Institutes for Biomedical Research, Cambridge, Massachusetts 02139, United States;* ⦿ orcid.org/0000-0002-1741-4862; Email: piro.siuti@novartis.com

Authors

Christopher J. Schwalen − *Global Discovery Chemistry, Novartis Institutes for Biomedical Research, Cambridge, Massachusetts 02139, United States*

Charles Babu − *Global Discovery Chemistry, Novartis Institutes for Biomedical Research, Cambridge, Massachusetts 02139, United States*

Swastik Phulera − *Chemical Biology and Therapeutics, Novartis Institutes for Biomedical Research, Cambridge, Massachusetts 02139, United States*

Qin Hao − *Pharmacokinetic Sciences, Novartis Institutes for Biomedical Research, Cambridge, Massachusetts 02139, United States*

Daniel Wall − *Pharmacokinetic Sciences, Novartis Institutes for Biomedical Research, Cambridge, Massachusetts 02139, United States*

David O. Nettleton − *Pharmacokinetic Sciences, Novartis Institutes for Biomedical Research, Cambridge, Massachusetts 02139, United States*

Complete contact information is available at:
https://pubs.acs.org/10.1021/acsomega.1c03707

Author Contributions

C.J.S, T.P.P, and P.S. devised the project and designed the experiments. NMR experimental design and analysis were performed by C.B. and C.J.S. Electrophysiology experiments were designed and executed by S.P. and C.J.S. Plasma stability testing was performed by Q.H. In vivo PK was performed by D.O.N. The manuscript was written by C.J.S. with support from T.P.P. and P.S. and input from all authors.

Notes

The authors declare no competing financial interest.

■ REFERENCES

(1) Arnison, P. G.; Bibb, M. J.; Bierbaum, G.; Bowers, A. A.; Bugni, T. S.; Bulaj, G.; Camarero, J. A.; Campopiano, D. J.; Challis, G. L.; Clardy, J.; Cotter, P. D.; Craik, D. J.; Dawson, M.; Dittmann, E.; Donadio, S.; Dorrestein, P. C.; Entian, K.-D.; Fischbach, M. A.; Garavelli, J. S.; Göransson, U.; Gruber, C. W.; Haft, D. H.; Hemscheidt, T. K.; Hertweck, C.; Hill, C.; Horswill, A. R.; Jaspars, M.; Kelly, W. L.; Klinman, J. P.; Kuipers, O. P.; Link, A. J.; Liu, W.; Marahiel, M. A.; Mitchell, D. A.; Moll, G. N.; Moore, B. S.; Müller, R.; Nair, S. K.; Nes, I. F.; Norris, G. E.; Olivera, B. M.; Onaka, H.; Patchett, M. L.; Piel, J.; Reaney, M. J. T.; Rebuffat, S.; Ross, R. P.; Sahl, H.-G.; Schmidt, E. W.; Selsted, M. E.; Severinov, K.; Shen, B.; Sivonen, K.; Smith, L.; Stein, T.; Süssmuth, R. D.; Tagg, J. R.; Tang, G.-L.; Truman, A. W.; Vederas, J. C.; Walsh, C. T.; Walton, J. D.; Wenzel, S. C.; Willey, J. M.; van der Donk, W. A. Ribosomally synthesized and post-translationally modified peptide natural products: overview and recommendations for a universal nomenclature. *Nat. Prod. Rep.* **2013**, *30*, 108−160.

(2) Jin, A.-H.; Muttenthaler, M.; Dutertre, S.; Himaya, S. W. A.; Kaas, Q.; Craik, D. J.; Lewis, R. J.; Alewood, P. F. Conotoxins: Chemistry and Biology. *Chem. Rev.* **2019**, *119*, 11510−11549.

(3) Postic, G.; Gracy, J.; Périn, C.; Chiche, L.; Gelly, J.-C. KNOTTIN: the database of inhibitor cystine knot scaffold after 10 years, toward a systematic structure modeling. *Nucleic Acids Res.* **2018**, *46*, D454−D458.

(4) Dongol, Y.; Caldas Cardoso, F.; Lewis, R. J. Spider Knottin Pharmacology at Voltage-Gated Sodium Channels and Their Potential to Modulate Pain Pathways. *Toxins* **2019**, *11*, 626.

(5) Chow, C. Y.; Chin, Y. K. Y.; Walker, A. A.; Guo, S.; Blomster, L. V.; Ward, M. J.; Herzig, V.; Rokyta, D. R.; King, G. F. Venom Peptides with Dual Modulatory Activity on the Voltage-Gated Sodium Channel NaV1. 1 Provide Novel Leads for Development of Antiepileptic Drugs. *ACS Pharmacol. Transl. Sci.* **2020**, *3*, 119−134.

(6) Kintzing, J. R.; Cochran, J. R. Engineered knottin peptides as diagnostics, therapeutics, and drug delivery vehicles. *Curr. Opin. Chem. Biol.* **2016**, *34*, 143−150.

(7) Moyer, B. D.; Murray, J. K.; Ligutti, J.; Andrews, K.; Favreau, P.; Jordan, J. B.; Lee, J. H.; Liu, D.; Long, J.; Sham, K.; Shi, L.; Stöcklin, R.; Wu, B.; Yin, R.; Yu, V.; Zou, A.; Biswas, K.; Miranda, L. P. Pharmacological characterization of potent and selective NaV1.7 inhibitors engineered from Chilobrachys jingzhao tarantula venom peptide JzTx-V. *PLoS One* **2018**, *13*, No. e0196791.

(8) Gao, X.; Stanger, K.; Kaluarachchi, H.; Maurer, T.; Ciepla, P.; Chalouni, C.; Franke, Y.; Hannoush, R. N. Cellular uptake of a cystine-knot peptide and modulation of its intracellular trafficking. *Sci. Rep.* **2016**, *6*, 35179.

(9) Murray, J. K.; Ligutti, J.; Liu, D.; Zou, A.; Poppe, L.; Li, H.; Andrews, K. L.; Moyer, B. D.; McDonough, S. I.; Favreau, P.; Stöcklin, R.; Miranda, L. P. Engineering Potent and Selective Analogues of GpTx-1, a Tarantula Venom Peptide Antagonist of the NaV1.7 Sodium Channel. *J. Med. Chem.* **2015**, *58*, 2299−2314.

(10) Lee, C. W.; Kim, S.; Roh, S. H.; Endoh, H.; Kodera, Y.; Maeda, T.; Kohno, T.; Wang, J. M.; Swartz, K. J.; Kim, J. I. Solution Structure and Functional Characterization of SGTx1, a Modifier of Kv2. 1 Channel Gating†,‡. *Biochemistry* **2004**, *43*, 890−897.

(11) Zhan, J.; Chen, X.; Wang, C.; Qiu, J.; Ma, F.; Wang, K.; Zheng, S. A fusion protein of conotoxin MVIIA and thioredoxin expressed in Escherichia coli has significant analgesic activity. *Biochem. Biophys. Res. Commun.* **2003**, *311*, 495−500.

(12) Klint, J. K.; Senff, S.; Saez, N. J.; Seshadri, R.; Lau, H. Y.; Bende, N. S.; Undheim, E. A. B.; Rash, L. D.; Mobli, M.; King, G. F. Production of Recombinant Disulfide-Rich Venom Peptides for Structural and Functional Analysis via Expression in the Periplasm of E. coli. *PLoS One* **2013**, *8*, No. e63865.

(13) Matsubara, F. H.; Gremski, L. H.; Meissner, G. O.; Constantino Lopes, E. S.; Gremski, W.; Senff-Ribeiro, A.; Chaim, O. M.; Veiga, S. S. A novel ICK peptide from the Loxosceles intermedia (brown spider) venom gland: Cloning, heterologous expression and immunological cross-reactivity approaches. *Toxicon* **2013**, *71*, 147−158.

(14) Pi, C.; Liu, J.; Wang, L.; Jiang, X.; Liu, Y.; Peng, C.; Chen, S.; Xu, A. Soluble expression, purification and functional identification of a disulfide-rich conotoxin derived from Conus litteratus. *J. Biotechnol.* **2007**, *128*, 184−193.

(15) Stanger, K.; Maurer, T.; Kaluarachchi, H.; Coons, M.; Franke, Y.; Hannoush, R. N. Backbone cyclization of a recombinant cystine-knot peptide by engineered Sortase A. *FEBS Lett.* **2014**, *588*, 4487−4496.

(16) Bernard, C.; Corzo, G.; Mosbah, A.; Nakajima, T.; Darbon, H. Solution Structure of Ptu1, a Toxin from the Assassin Bug Peirates turpis That Blocks the Voltage-Sensitive Calcium Channel N-Type. *Biochemistry* **2001**, *40*, 12795−12800.

(17) Bi, T.; Li, Y.; Shekhtman, A.; Camarero, J. A. In-cell production of a genetically-encoded library based on the θ-defensin RTD-1 using a bacterial expression system. *Bioorg. Med. Chem.* **2018**, *26*, 1212−1219.

(18) Jagadish, K.; Camarero, J. A., Recombinant Expression of Cyclotides Using Split Inteins. In *Split Inteins: Methods and Protocols*, Mootz, H. D., Ed. Springer New York: New York, NY, 2017, 41−55.

(19) Jagadish, K.; Gould, A.; Borra, R.; Majumder, S.; Mushtaq, Z.; Shekhtman, A.; Camarero, J. A. Recombinant Expression and Phenotypic Screening of a Bioactive Cyclotide Against α-Synuclein-Induced Cytotoxicity in Baker's Yeast. *Angew. Chem., Int. Ed.* **2015**, *54*, 8390−8394.

(20) Berndt, C.; Lillig, C. H.; Holmgren, A. Thioredoxins and glutaredoxins as facilitators of protein folding. *Biochim. Biophys. Acta, Mol. Cell Res.* **2008**, *1783*, 641−650.

(21) Bessette, P. H.; Aslund, F.; Beckwith, J.; Georgiou, G. Efficient folding of proteins with multiple disulfide bonds in the Escherichia coli cytoplasm. *Proc. Natl. Acad. Sci. U. S. A.* **1999**, *96*, 13703−13708.

(22) de Marco, A. Strategies for successful recombinant expression of disulfide bond-dependent proteins in Escherichia coli. *Microb. Cell Fact.* **2009**, *8*, 26.

(23) Lobstein, J.; Emrich, C. A.; Jeans, C.; Faulkner, M.; Riggs, P.; Berkmen, M. SHuffle, a novel Escherichia coli protein expression strain capable of correctly folding disulfide bonded proteins in its cytoplasm. *Microb. Cell Fact.* **2012**, *11*, 753.

(24) Lauber, T.; Marx, U. C.; Schulz, A.; Kreutzmann, P.; Rösch, P.; Hoffmann, S. Accurate Disulfide Formation in Escherichia coli: Overexpression and Characterization of the First Domain (HF6478) of the Multiple Kazal-Type Inhibitor LEKTI. *Protein Expression Purif.* **2001**, *22*, 108−112.

(25) García-Santamarina, S.; Boronat, S.; Calvo, I. A.; Rodríguez-Gabriel, M.; Ayté, J.; Molina, H.; Hidalgo, E. Is Oxidized Thioredoxin a Major Trigger for Cysteine Oxidation? Clues from a Redox Proteomics Approach. *Antioxid. Redox Signaling* **2013**, *18*, 1549−1556.

(26) Stewart, E. J.; Aslund, F.; Beckwith, J. Disulfide bond formation in the Escherichia coli cytoplasm: an in vivo role reversal for the thioredoxins. *EMBO J.* **1998**, *17*, 5543−5550.

(27) Holmgren, A. Thioredoxin and Glutaredoxin Systems. *J. Biol. Chem.* **1989**, *264*, 13963−13966.

(28) Kong, B.; Guo, G. L. Soluble Expression of Disulfide Bond Containing Proteins FGF15 and FGF19 in the Cytoplasm of Escherichia coli. *PLoS One* **2014**, *9*, No. e85890.

(29) Manta, B.; Boyd, D.; Berkmen, M. *Disulfide Bond Formation in the Periplasm of Escherichia coli*. EcoSal Plus 2019, *8* (2), DOI: 10.1128/ecosalplus.ESP-0012-2018.

(30) Takahashi, H.; Kim, J. I.; Min, H. J.; Sato, K.; Swartz, K. J.; Shimada, I. Solution structure of hanatoxin1, a gating modifier of voltage-dependent K+ channels: common surface features of gating modifier toxins11Edited by PE Wright. *J. Mol. Biol.* **2000**, *297*, 771−780.

(31) Dai, Q.; Liu, F.; Zhou, Y.; Lu, B.; Yu, F.; Huang, P. The Synthesis of SO-3, a Conopeptide with High Analgesic Activity Derived from Conus striatus. *J. Nat. Prod.* **2003**, *66*, 1276−1279.

(32) King, G., *Venoms to Drugs: Venom as a Source for the Development of Human Therapeutics*; Royal Society of Chemistry: 2015.

(33) Bernard, C.; Corzo, G.; Mosbah, A.; Nakajima, T.; Darbon, H. Solution Structure of Ptu1, a Toxin from the Assassin BugPeirates turpisThat Blocks the Voltage-Sensitive Calcium Channel N-Type†. *Biochemistry* **2001**, *40*, 12795−12800.

(34) Kohno, T.; Kim, J. I.; Kobayashi, K.; Kodera, Y.; Maeda, T.; Sato, K. Three-Dimensional Structure in Solution of the Calcium Channel Blocker omega.-Conotoxin MVIIA. *Biochemistry* **1995**, *34*, 10256−10265.

(35) Minassian, N. A.; Gibbs, A.; Shih, A. Y.; Liu, Y.; Neff, R. A.; Sutton, S. W.; Mirzadegan, T.; Connor, J.; Fellows, R.; Husovsky, M.; Nelson, S.; Hunter, M. J.; Flinspach, M.; Wickenden, A. D. Analysis of the Structural and Molecular Basis of Voltage-sensitive Sodium Channel Inhibition by the Spider Toxin Huwentoxin-IV (μ-TRTX-Hh2a). *J. Biol. Chem.* **2013**, *288*, 22707−22720.

(36) Oliveira, J. S.; Redaelli, E.; Zaharenko, A. J.; Cassulini, R. R.; Konno, K.; Pimenta, D. C.; Freitas, J. C.; Clare, J. J.; Wanke, E. Binding Specificity of Sea Anemone Toxins to Nav1. 1−1.6 Sodium Channels. *J. Biol. Chem.* **2004**, *279*, 33323−33335.

(37) Wunderer, G.; Fritz, H.; Wachter, E.; Machleidt, W. Amino-Acid Sequence of a Coelenterate Toxin: Toxin II from Anemonia sulcata. *Eur. J. Biochem.* **1976**, *68*, 193−198.

(38) Ulbricht, W. Sodium channel inactivation: molecular determinants and modulation. *Physiol. Rev.* **2005**, *85*, 1271−1301.

(39) Moran, Y.; Cohen, L.; Kahn, R.; Karbat, I.; Gordon, D.; Gurevitz, M. Expression and Mutagenesis of the Sea Anemone Toxin Av2 Reveals Key Amino Acid Residues Important for Activity on Voltage-Gated Sodium Channels†. *Biochemistry* **2006**, *45*, 8864−8873.

(40) Bell, D. C.; Karratt-Vellatt, A.; Surade, S.; Luetkens, T.; Masters, E. W.; Sørensen, N. M.; Butt, N.; McCafferty, J. Knotbodies: A New Generation of Ion Channel Therapeutic Biologics Created by Fusing Knottin Toxins into Antibodies. *Biophys. J.* **2018**, *114*, 203a.

(41) Kimura, R. H.; Wang, L.; Shen, B.; Huo, L.; Tummers, W.; Filipp, F. V.; Guo, H. H.; Haywood, T.; Abou-Elkacem, L.; Baratto, L.; Habte, F.; Devulapally, R.; Witney, T. H.; Cheng, Y.; Tikole, S.; Chakraborti, S.; Nix, J.; Bonagura, C. A.; Hatami, N.; Mooney, J. J.; Desai, T.; Turner, S.; Gaster, R. S.; Otte, A.; Visser, B. C.; Poultsides, G. A.; Norton, J.; Park, W.; Stolowitz, M.; Lau, K.; Yang, E.; Natarajan, A.; Ilovich, O.; Srinivas, S.; Srinivasan, A.; Paulmurugan, R.; Willmann, J.; Chin, F. T.; Cheng, Z.; Iagaru, A.; Li, F.; Gambhir, S. S. Evaluation of integrin alphavbeta6 cystine knot PET tracers to detect cancer and idiopathic pulmonary fibrosis. *Nat. Commun.* **2019**, *10*, 4673.

(42) Kikuchi, K.; Sugiura, M.; Kimura, T. High Proteolytic Resistance of Spider-Derived Inhibitor Cystine Knots. *Int. J. Pept.* **2015**, *2015*, No. 537508.

(43) Wilson, D.; Daly, N. Venomics: A Mini-Review. *High-Throughput* **2018**, *7*, 19.

(44) Lu, S.; Wu, Y.; Li, J.; Meng, X.; Hu, C.; Zhao, Y.; Wu, C. Directed Disulfide Pairing and Folding of Peptides for the De Novo Development of Multicyclic Peptide Libraries. *J. Am. Chem. Soc.* **2020**, *142*, 16285.

(45) Daly, N. L.; Clark, R. J.; Craik, D. J. Disulfide Folding Pathways of Cystine Knot Proteins. *J. Biol. Chem.* **2003**, *278*, 6314−6322.

(46) Reinwarth, M.; Glotzbach, B.; Tomaszowski, M.; Fabritz, S.; Avrutina, O.; Kolmar, H. Oxidative Folding of Peptides with Cystine-Knot Architectures: Kinetic Studies and Optimization of Folding Conditions. *ChemBioChem* **2013**, *14*, 137−146.

(47) Reinwarth, M.; Nasu, D.; Kolmar, H.; Avrutina, O. Chemical Synthesis, Backbone Cyclization and Oxidative Folding of Cystine-knot Peptides — Promising Scaffolds for Applications in Drug Design. *Molecules* **2012**, *17*, 12533−12552.

(48) Marley, J.; Lu, M.; Bracken, C. A method for efficient isotopic labeling of recombinant proteins. *J. Biomol. NMR* **2001**, *20*, 71−75.

(49) McCarthy, S.; Robinson, J.; Thalassinos, K.; Tabor, A. B. A Chemical Biology Approach to Probing the Folding Pathways of the Inhibitory Cystine Knot (ICK) Peptide ProTx-II. *Front. Chem.* **2020**, *8*, 228.